



## RESEARCH ARTICLE

View Article Online  
View Journal | View IssueCite this: *Mater. Chem. Front.*,  
2019, 3, 1335

# Redox-responsive fluorescent AIE bioconjugate with aggregation enhanced retention features for targeted imaging reinforcement and selective suppression of cancer cells†

Ling Yang,<sup>a</sup> Wen Fang,<sup>a</sup> Yuxiao Ye,<sup>b</sup> Zhengke Wang,<sup>b</sup> \*<sup>a</sup> Qiaoling Hu<sup>a</sup> and Ben Zhong Tang \*<sup>c</sup>

Considering the distinctions of cancer cell microenvironments, smart systems with stimulus-triggered features have become increasingly popular nowadays. These smart systems are regarded as efficient approaches for targeted cancer cell imaging and selective tumoricidal therapy. On account of the highly reductive micro-environment in tumor tissues, a redox-responsive fluorescent AIE bioprobe based on a disulfide bond is designed and synthesized. This AIE bioprobe possesses excellent water dispersibility and nano-size stability under physiological conditions. Under the reductive microenvironment of tumor cells, the water dispersibility of the AIE probe becomes worse owing to the cleavage of carboxyl groups. The dispersibility alteration further induces the aggregation of AIE nanoparticles and enhances intracellular retention, allowing for targeted imaging reinforcement and selective suppression of cancer cells.

Received 4th April 2019,  
Accepted 29th April 2019

DOI: 10.1039/c9qm00216b

rsc.li/frontiers-materials

## Introduction

Cancer, the greatest threat to human health, causes millions of deaths worldwide and the incidence of cancer is continuously increasing.<sup>1</sup> Tremendous endeavors have been devoted to developing effective techniques and anticancer drugs for diagnosis and treatment.<sup>2–5</sup> Early diagnosis and therapy of cancer before its metastasis are of great significance for its cure, while early diagnosis is difficult to carry out due to the small size of the tumor. Fluorescent bioprobes can realize real-time monitoring with high resolution, which endows them with unique superiorities in the diagnosis of cancer at an early stage. Thus, many fluorophores have been designed for the early-stage diagnosis of cancer.<sup>6</sup>

The development of fluorescence bioprobes, such as fluorescent polymers,<sup>7,8</sup> inorganic nanoparticles,<sup>9</sup> organic dyes,<sup>10–12</sup> and quantum dots (QDs),<sup>13</sup> which provide alternatives for cell imaging and tracing, has recently attracted a great deal of research attention.

These fluorescence bioprobes have significant applications in the monitoring and visualization of biological features, and the diagnosis and tracking of many diseases in living systems. Among these approaches, fluorescence bioprobes with the aggregation-induced emission characteristic (AIEgens) exhibit prominent performances, such as adjustable emission brightness *via* regulating the aggregation form, high resistance to photobleaching and easy modification of specific groups.<sup>14–16</sup> These AIEgens could serve as superior agents for biological process monitoring<sup>17–21</sup> and disease theranostics.<sup>22–25</sup> Particularly, designing intelligent AIE bioprobes that can respond to stimuli in tumour microenvironments opens new avenues to the advancement of cancer imaging and therapy, providing comprehensive insight into pathogenesis mechanisms and a precise guide in theranostics.<sup>26–29</sup>

As for the stimuli in tumour microenvironments, reductive-responsiveness has been investigated in controlled drug delivery for better cancer targeting and treatment.<sup>30–33</sup> This is based on the fact that the microenvironment in tumour tissues is more reductive than in the normal tissues, with about a 4-fold elevated concentration of glutathione (γ-glutamyl-cysteinyl-glycine, GSH), which could cleave the disulfide bond through the thiol–disulfide exchange reaction.<sup>31,34</sup> Moreover, an alteration of intracellular GSH level is closely tied with many health problems such as cancer, cardiovascular diseases, diabetes, neurological disorder and ageing.<sup>30,35</sup> Enthusiastic research on GSH-triggered drug delivery systems has inspired scientists to explore efficient GSH-responsive AIE bioprobes that are capable of targeted cancer cell

<sup>a</sup> MOE Key Laboratory of Macromolecular Synthesis and Functionalization, Department of Polymer Science and Engineering, Zhejiang University, Hangzhou 310027, China. E-mail: wangzk@zju.edu.cn

<sup>b</sup> School of Materials Science and Engineering, New South Wales University, Sydney 2052, Australia

<sup>c</sup> Department of Chemistry, Hong Kong University of Science and Technology, Clear Water Bay, Hong Kong 999077, China. E-mail: tangbenz@ust.hk

† Electronic supplementary information (ESI) available: Synthesis procedures, <sup>1</sup>H NMR spectra, fluorescence spectra, size stability, AIE behaviour, cell viability, flow cytometric analysis, etc. See DOI: 10.1039/c9qm00216b

imaging, selective cellular tracing and monitoring intricate biological processes.<sup>36,37</sup> However, their GSH-responsiveness is realized *via* the cleavage of the link between AIE molecules and a hydrophilic polymer chain. And the cleaved AIE small molecules are likely to leak, which largely restricts their biomedical applications.<sup>38</sup>

Water dispersibility, size stability and leakage-free properties are vital elements for the biocompatibility and tracing capability of AIE bioprobes.<sup>38–40</sup> Conjugating AIE molecules onto hydrophilic polymers to self-assemble into nanoparticles (NPs) is a prominent approach to improve their water dispersibility retention ability. NPs with a diameter between 30 and 200 nm can be easily internalized through endocytosis, and they have been widely designed to realize various inspiring functions *in vivo*, especially for the diagnosis and treatment of cancer.<sup>41–43</sup> Furthermore, cellular uptake and enhanced retention of small NPs in tumor sites could be achieved by stimulated NP aggregation in certain microenvironments. To date, a few studies have focused on the stimulus-triggered intracellular retention enhancement effect and subsequent aggregation induced emission reinforcement of AIE NP bioprobes.<sup>44,45</sup>

This contribution reports a rational design and synthesis of redox-responsive AIE bioconjugate NPs based on the disulfide bond for targeted imaging reinforcement and selective suppression of cancer cells. The NP bioprobe (TPE-CS-ss-COOH, shortened as TCSC, see Fig. 1) consists of a chitosan (CS) polymer chain attached with a large number of tetraphenylethylene (TPE)

units and disulfide-linked carboxyl groups. In 10  $\mu\text{M}$  DTT solution, which mimics physiological conditions, TCSC exhibits excellent water dispersibility, nano-size stability and dispersive fluorescent emission. Upon exposure to 10 mM DTT solution, which mimics a tumor reductive microenvironment,<sup>46,47</sup> the disulfide bonds of the NPs are cleaved *via* the thiol–disulfide exchange reaction. Consequent detachment of the carboxyl groups induces worse water dispersibility and causes further aggregation of TPE-CS. The augmented aggregation would not only enhance the intracellular retention of NPs, but also elevate the emission brightness and contrast to some extent. Furthermore, the GSH-triggered aggregation-enhanced retention effect makes cellular tracing and monitoring the biological behaviors of cancer cells feasible. It is found that the TCSC NP bioprobes could also selectively suppress the propagation of cancer cells. To the best of our knowledge, this is the first report on the synthesis and application of GSH-triggered AIE fluorescent reinforcement and retention enhancement NP bioprobes, which will inspire more exciting research in the fields of AIE bioimaging and precise cancer theranostics.

## Experimental section

### Materials and instruments

All the chemicals and reagents were purchased from Aldrich and Sinopharm Chemical Reagent Co., Ltd and used without further purification, unless specified otherwise. Chitosan ( $M_n = 2.52 \times 10^4$ ) was supplied by the Qingdao Haihui Bio-engineering Co., Ltd (Qingdao, China) with 83.5% degree of deacetylation. TPE-ITC was synthesized according to our previous research.<sup>21</sup> DMEM containing 10% fetal bovine serum and antibiotics (100 units  $\text{mL}^{-1}$  penicillin and 100  $\mu\text{g mL}^{-1}$  streptomycin) was purchased from Geno Biopharmaceutical Technology Co., Ltd (Hangzhou, China). MitoTracker<sup>®</sup> Red, FITC Annexin V and Propidium Iodide (PI) were obtained from Invitrogen Corp. The synthesis, apparatus, cytotoxicity and live cell imaging procedures are described in the ESI.†

## Results and discussion

### Molecular design and AIE properties

The disulfide-linked carboxyl chitosan (CS-ss-COOH) was first synthesized *via* amidation between the terminal carboxyl groups of dithiodipropionic acid and amino groups of CS. TPE with isothiocyanate groups (TPE-ITC) was then conjugated with CS-ss-COOH to afford TCSC (Fig. 1a). The detailed synthetic routes and characterization (<sup>1</sup>H NMR spectrum) are shown in Fig. 1a and Fig. S1 in the ESI.† It was calculated from the <sup>1</sup>H NMR spectrum that approximately 22 ss-COOH units are conjugated to one CS chain on average and there are roughly 11 TPE groups on one CS chain on average. The solid powder of TCSC emits a strong greenish-blue light (inset picture in Fig. 1a) when excited by UV light. The high fluorescent emission in the solid state confirms its AIE characteristics, which differ from the traditional aggregation caused quenching (ACQ) of fluorescent dyes.

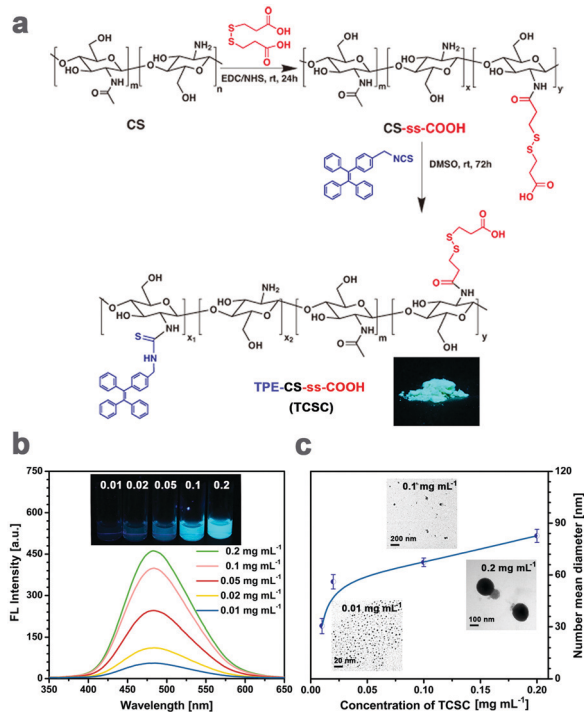


**Fig. 1** Molecular design and AIE properties of TCSC. (a) Synthetic route of the NP probes of TCSC. Inset: TCSC solid powder under UV illumination; (b) fluorescence spectrum of the TCSC aqueous solution at different concentrations. Inset: Photographs of TCSC solutions excited by UV light; (c) hydrodynamic diameter of TCSC aqueous solution at different concentrations. Inset: TEM images of the corresponding concentrations.

The fluorescence (FL) intensity of TCSC solutions with different ethanol (poor solvent)/H<sub>2</sub>O (good solvent) ratios was utilized to further verify the AIE effect of the TCSC bioconjugate (Fig. S2, ESI<sup>†</sup>). It is obvious that the FL intensity (emission around 480 nm) increases with the increase of the poor solvent content. In addition, FL intensity and the corresponding diameter of the TCSC aqueous solutions with different concentrations (0.01, 0.02, 0.05, 0.1, and 0.2 mg mL<sup>-1</sup>) were measured by using FL spectroscopy, Dynamic light scattering (DLS) and TEM (Fig. 1). The DLS and TEM results suggest that the hydrodynamic diameters of the TCSC NPs are of nano-size in aqueous media (30–100 nm) and TCSC NPs appear to possess excellent water dispersibility and nano-size stability (Fig. S3 and S4b, ESI<sup>†</sup>). The mechanism of TCSC NP formation in the aqueous solution can be ascribed to the self-assembly of TCSC polymer chains, with hydrophobic fluorophore TPE as the interior core and the exposed hydrophilic carboxyl groups as the exterior layers. With an increase in the concentration (0.01 to 0.2 mg mL<sup>-1</sup>) and degree of labelling (2.16 mol% to 8.63 mol%), TCSC NPs exhibit augmented luminance and a slightly red-shifted emission peak, indicating tighter packing and restricted intramolecular rotation of TPE aggregates in the core (Fig. 1c and Fig. S4a, ESI<sup>†</sup>).<sup>48</sup>

### Redox-induced aggregation of TCSC bioprobes

To verify that TCSC can switch the distribution form of the NPs in response to a highly reductive microenvironment, the FL spectrum and the hydrodynamic diameter changes of the NP bioprobes over time in 10 mM DTT were investigated and their transition tendencies are presented in Fig. 2. As shown in Fig. 2a and b, upon incubation of TCSC NPs in 10 mM DTT, the FL intensity of the mixture increases gradually as time elapses. Correspondingly, the hydrodynamic diameters of the TCSC bioprobes exhibit a positive correlation with incubation time (from 40 nm at 0 h to 200 nm at 36 h, and several  $\mu$ m at 60 h, see Fig. 2c and d). These results manifest the occurrence

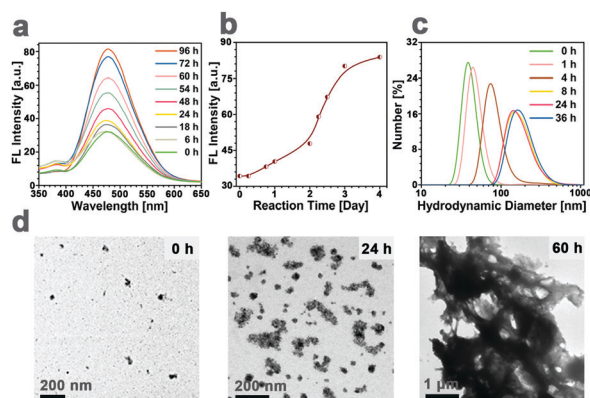
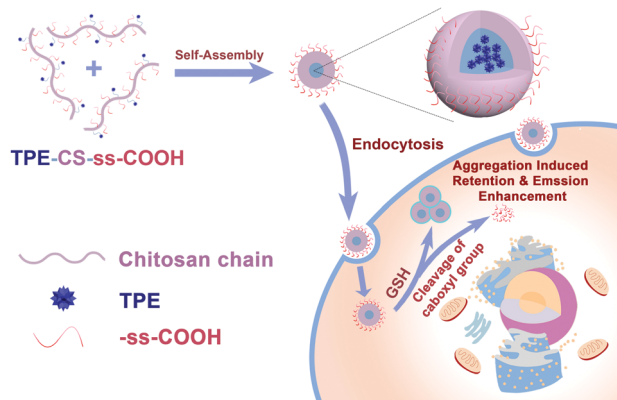


**Fig. 2** Redox-responsive properties of TCSC bioprobes. (a) FL spectrum of TCSC after different incubation periods in 10 mM DTT; (b) FL intensity changes of TCSC bioprobes incubated in 10 mM DTT over time; (c) hydrodynamic diameter distribution changes of TCSC after different reaction times in 10 mM DTT; (d) TEM images of the corresponding nanoparticles after different incubation periods.



**Scheme 1** Schematic illustration of TPE-CS-ss-COOH as a redox-responsive NP bioprobe for GSH-triggered aggregation enhanced retention and targeted imaging reinforcement of cancer cells.

of the redox-responsive cleavage of carboxyl groups on TCSC in the reductive microenvironment.

### Redox-induced imaging reinforcement and selective suppression of cancer cells

Considering the goal of targeted cellular tracing and biomedical applications of TCSC NPs, it is noteworthy to explore the cytotoxicity of the NP bioprobes against both cancer cells and normal cells. MTT cell viability assays were conducted after 1 d, 3 d, and 5 d incubation of HeLa, HepG2, MCF-7 and FIB with the TCSC NP bioprobes. As shown in Fig. S5 (ESI<sup>†</sup>), TCSC at a concentration of 0.1 mg mL<sup>-1</sup> shows relatively higher cytotoxicity to cancer cells (HeLa, HepG2 and MCF-7, with a higher GSH content) than

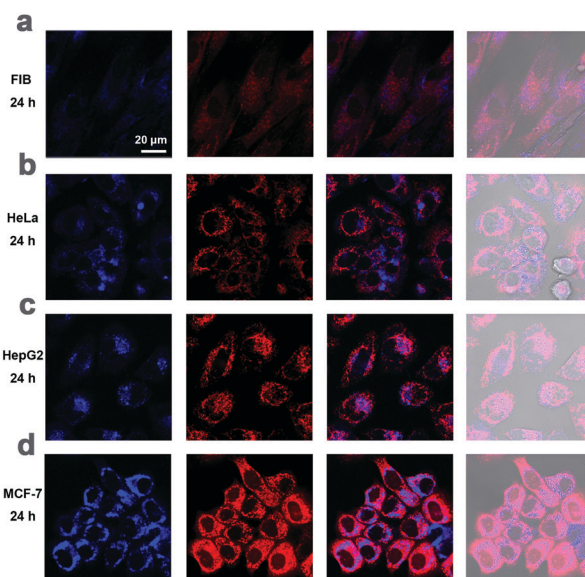


**Fig. 3** Confocal laser scanning microscopy (CLSM) images of different cells stained by 0.1 mg mL<sup>-1</sup> TCSC for 24 h, and then stained by MitoTracker<sup>®</sup> Red CMXRos for TCSC NP localization. (a) FIB; (b) HeLa; (c) HepG2; (d) MCF-7. First column: TCSC particles (blue); second column: mitochondria (red); third column: merge images of two fluorescence channels; and fourth column: with corresponding bright field channel images, respectively.

normal FIB cells, especially for relatively long-term cellular retention at 5 days. These results reveal that the difference in the reductive microenvironments of cancer and normal cells largely affects the cytotoxicity of the TCSC NP bioprobes. The highly reductive microenvironment of cancer cells can induce the aggregation and size augmentation of TCSC NPs, further causing the suppression of cancer cells.<sup>49,50</sup>

On account of this fact, it is reasonable to hypothesize that the cleavage of carboxyl groups on TCSC in a reductive intracellular microenvironment can not only reinforce its aggregation and FL intensity in cancer cells, but also enhance the intracellular retention of the NPs owing to the augmentation of particle size (Scheme 1). The GSH-triggered augmentation of particle size contributes to the long-term retention and selective suppression of cancer cells. The internalized TCSC NPs function as supramolecular aggregates, and they do not undergo exocytosis once internalized, accounting for their remarkable leakage-free staining behaviors.<sup>24</sup> Consequently, the TCSC NPs could hardly be excreted *via* exocytosis and they maintained their aggregated form in the reductive microenvironment, leading to the suppression of cancer cells.

In order to authenticate this hypothesis, the utilization of TCSC NP bioprobes for targeted cancer cell imaging was conducted

using confocal laser scanning microscopy (CLSM). After incubation with TCSC (0.1 mg mL<sup>-1</sup>) in the culture medium for 24 h at 37 °C, HeLa, HepG2, MCF-7 and FIB cells were observed, respectively. After a 24 h incubation period, TCSC NPs are internalized into the cells and appear to locate in the cytoplasm region. Merely weak fluorescence can be observed inside the FIB normal cells, while the cancer cells (HeLa, HepG2, and MCF-7) present apparently stronger FL emission than that of the normal cells (Fig. 3). Besides, the statistical results for average FL intensity per cell (Fig. S6, ESI<sup>†</sup>) corroborate the hypothesis that the TCSC NP bioprobes can serve as a redox-responsive AIE bioprobe for targeted cancer cell imaging reinforcement.

### Mechanism of redox-induced aggregation enhanced retention (AER) effect

For the purpose of figuring out the mechanism for the different cytotoxicity and imaging effect of TCSC on cancer cells and normal cells, cellular tracing and corresponding apoptosis measurements were carried out on FIB and HeLa for comparison. The living HeLa cells stained by TCSC emit intensively for 5 generations (Fig. 4a), while much weaker emission is noticed for the stained FIB living cells (Fig. 4b). Additionally, there exist different staining regions for the two cells, shown as a more

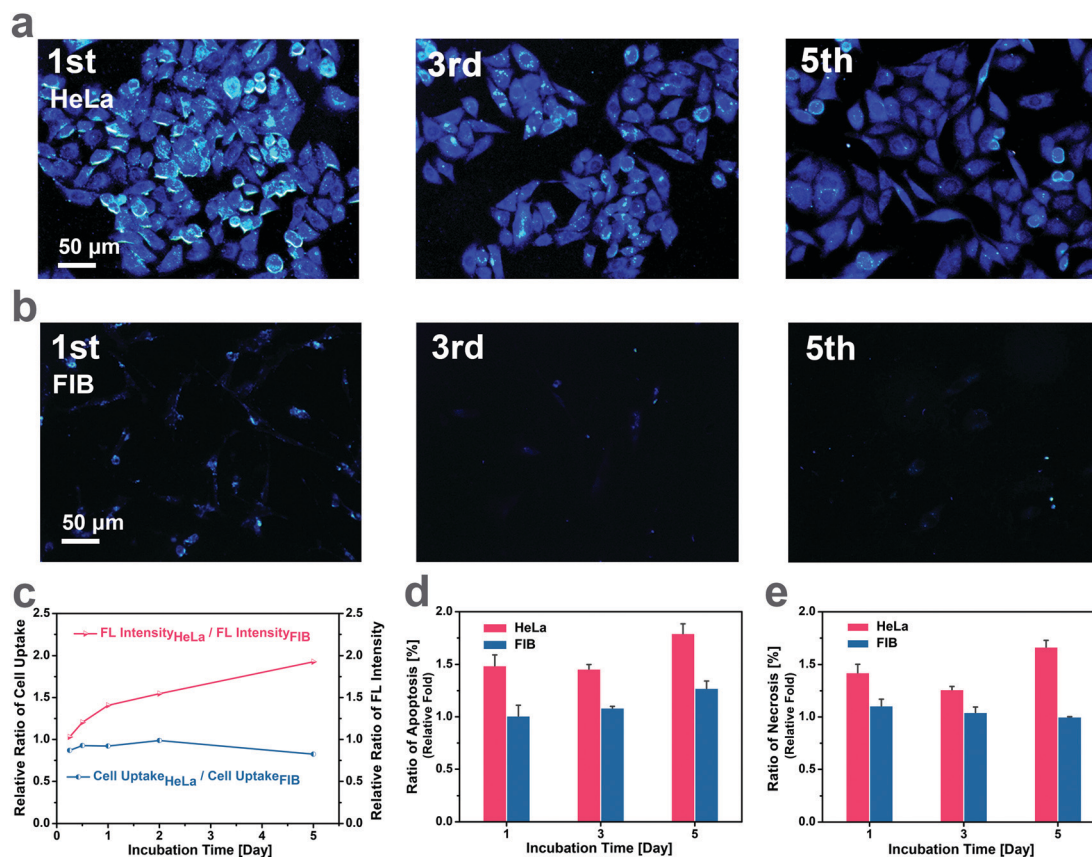


**Fig. 4** Mechanism of redox-induced aggregation enhanced retention (AER) effect. Cellular tracing of (a) HeLa cancer cells and (b) FIB normal cells by 0.1 mg mL<sup>-1</sup> TCSC at different passages; (c) relative ratio of cell uptake amount for HeLa and FIB (Cell Uptake<sub>HeLa</sub>/Cell Uptake<sub>FIB</sub>, blue line) and relative ratio of FL intensity for HeLa and FIB (FL Intensity<sub>HeLa</sub>/FL Intensity<sub>FIB</sub>, red line) at different incubation times determined by using a UV standard curve and fluorescence spectrum, respectively; (d) ratio of apoptosis and (e) necrosis for HeLa and FIB relative to the blank control at different incubation times determined by using flow cytometry.

dispersed distribution of TCSC NP bioprobes within the FIB cells, and evident clustered regions of TCSC NP bioprobes appearing inside the HeLa cells. For the purpose of confirming that the higher FL intensity of HeLa cells is unrelated to the probable higher TCSC NP intake caused by cellular activity differences, different cellular seeding densities were applied to HeLa cells and FIB cells to realize a lower TCSC uptake for the HeLa cells. It is noteworthy that the HeLa cells present a relatively higher FL intensity with a comparatively lower TCSC NP intake compared to the FIB cells (Fig. 4c). This phenomenon can be interpreted as follows: the highly reductive microenvironment inside HeLa triggers the cleavage of the hydrophilic shells of the TCSC NPs, further inducing core aggregation and emission reinforcement of the AIE bioprobes. Tangible proof is provided by some especially bright dots and clusters emerging in the HeLa cells (Fig. 4a). Besides, these especially bright dots and clusters tend to appear regularly inside round cells, which is commonly regarded as a sign of apoptosis. With the extension of the staining time, there is clearly a descending tendency in the quantity of cells and an ascending probability for the appearance of round cells with especially bright dots, demonstrating the suppression of HeLa cells.

The results of the apoptosis measurements determined by flow cytometry indicate that the uptake of TCSC NPs induces the apoptosis of HeLa cells, which further leads to their relatively high ratio of apoptosis and necrosis during long time incubation (Fig. 4d and e). Although there exists an understandable inconsistency in cell viability value owing to the methodological difference, the results and tendency of the flow cytometry assays are in high accordance with the cytotoxicity trend of MTT assays mentioned before. TCSC NPs could suppress the propagation and increase the apoptosis/necrosis ratio of HeLa cells. The redox-induced aggregation and size augmentation of the TCSC NPs can be regarded as the specific cause of the TCSC NP inhibition activity on cancer cells. It can be elucidated that the cleaving of carboxyl residues in cancer cells results in the ulterior aggregation of the TCSC NPs. The enhanced TCSC NP aggregation further induces the retention enhancement (AER) and emission reinforcement of the AIE bioprobes, and the long-term retention and accumulation of large particles finally contribute to the cytotoxicity toward and apoptosis of cancer cells.

## Conclusion

In summary, a new design strategy for AIE bioprobes that can respond to a tumor reductive microenvironment is reported. The NP bioprobe possesses excellent water dispersibility, nano-size stability, and dispersive fluorescent emission under physiological conditions. In the highly reductive microenvironment with 10 mM DTT, the NP bioprobe sacrifices its dispersity as a result of carboxyl group detachment, inducing the further aggregation of TCSC NPs and augmentation in both particle size and luminous intensity. *In vitro* experiments demonstrate that there exist significant distinctions between normal cells and cancer cells after incubation with TCSC, in terms of fluorescence intensity, staining regions, retention time and cytotoxicity. Flow cytometry measurements verify

that the aggregated TCSC NPs trigger the apoptosis of HeLa cells and contribute to their necrosis. All these results suggest that the TCSC NP bioprobes can be utilized for targeted cancer cell imaging reinforcement and selective suppression of cancer cells, making them superior agents for biological process monitoring and cancer theranostics. However, there still exists some intrinsic weakness for blue-emitting fluorescent systems, especially due to their restriction *in vivo* imaging applications. This work just explores the tip of the iceberg. Development of a red-emitting AIE bioconjugate with stimulus-triggered aggregation enhanced retention features would be promising for cancer diagnosis and therapy *in vivo*.

## Conflicts of interest

The authors declare no competing financial interests.

## Acknowledgements

This work was financially supported by the National Natural Science Foundation of China (No. 51873187), the National Key Research and Development Program of China (No. 2017YFE0117700 and 2018YFC1004803) and 2018 Zhejiang University Academic Award for Outstanding Doctoral Candidates (No. 2018082).

## Notes and references

- 1 D. Hanahan and R. A. Weinberg, *Cell*, 2011, **144**, 646–674.
- 2 S. S. Gambhir, *Nat. Rev. Cancer*, 2002, **2**, 683–693.
- 3 D. J. Brenner and E. J. Hall, *N. Engl. J. Med.*, 2007, **357**, 2277–2284.
- 4 M. D. Fox and M. E. Raichle, *Nat. Rev. Neurosci.*, 2007, **8**, 700–711.
- 5 J. E. Kennedy, *Nat. Rev. Cancer*, 2005, **5**, 321–327.
- 6 J. Mei, N. L. C. Leung, R. T. K. Kwok, J. W. Y. Lam and B. Z. Tang, *Chem. Rev.*, 2015, **115**, 11718–11940.
- 7 K. Wang, X. Zhang, X. Zhang, C. Ma, Z. Li, Z. Huang, Q. Zhang and Y. Wei, *Polym. Chem.*, 2015, **6**, 4455–4461.
- 8 S. R. Meech, *Chem. Soc. Rev.*, 2009, **38**, 2922–2934.
- 9 K. Zhou, Y. Zhang, Z. Xia and W. Wei, *Nanotechnology*, 2016, **27**, 275101.
- 10 J. Niu, J. Fan, X. Wang, Y. Xiao, X. Xie, X. Jiao, C. Sung and B. Tang, *Anal. Chem.*, 2017, **89**, 7210–7215.
- 11 J. Shi, Q. Deng, C. Wan, M. Zheng, F. Huang and B. Tang, *Chem. Sci.*, 2017, **8**, 6188–6195.
- 12 J. Shi, Q. Deng, Y. Li, M. Zheng, Z. Chai, C. Wan, Z. Zheng, L. Li, F. Huang and B. Tang, *Anal. Chem.*, 2018, **90**, 13775–13782.
- 13 X. Michalet, F. F. Pinaud, L. A. Bentolila, J. M. Tsay, S. Doose, J. J. Li, G. Sundaresan, A. M. Wu, S. S. Gambhir and S. Weiss, *Science*, 2005, **307**, 538–544.
- 14 J. D. Luo, Z. L. Xie, J. W. Y. Lam, L. Cheng, H. Y. Chen, C. F. Qiu, H. S. Kwok, X. W. Zhan, Y. Q. Liu, D. B. Zhu and B. Z. Tang, *Chem. Commun.*, 2001, 1740–1741.

- 15 M. Wang, G. X. Zhang, D. Q. Zhang, D. B. Zhu and B. Tang, *J. Mater. Chem.*, 2010, **20**, 1858–1867.
- 16 Y. Hong, J. W. Y. Lam and B. Z. Tang, *Chem. Soc. Rev.*, 2011, **40**, 5361–5388.
- 17 G. Feng, Y. Yuan, H. Fang, R. Zhang, B. Xing, G. Zhang, D. Zhang and B. Liu, *Chem. Commun.*, 2015, **51**, 12490–12493.
- 18 Y. Yuan, R. T. K. Kwok, G. Feng, J. Liang, J. Geng, B. Z. Tang and B. Liu, *Chem. Commun.*, 2014, **50**, 295–297.
- 19 M. Gao, C. K. Sim, C. W. T. Leung, Q. Hu, G. Feng, F. Xu, B. Z. Tang and B. Liu, *Chem. Commun.*, 2014, **50**, 8312–8315.
- 20 J. Chen, M. Gao, L. Wang, S. Li, J. He, A. Qin, L. Ren, Y. Wang and B. Z. Tang, *ACS Appl. Mater. Interfaces*, 2018, **10**, 11436–11442.
- 21 Z. Wang, S. Chen, J. W. Lam, W. Qin, R. T. Kwok, N. Xie, Q. Hu and B. Z. Tang, *J. Am. Chem. Soc.*, 2013, **135**, 8238–8245.
- 22 X. Gao, G. Feng, P. N. Manghnani, F. Hu, N. Jiang, J. Liu, B. Liu, J. Z. Sun and B. Z. Tang, *Chem. Commun.*, 2017, **53**, 1653–1656.
- 23 K. Han, S. B. Wang, Q. Lei, J. Y. Zhu and X. Z. Zhang, *ACS Nano*, 2015, **9**, 10268–10277.
- 24 Y. Yu, C. Feng, Y. Hong, J. Liu, S. Chen, K. M. Ng, K. Q. Luo and B. Z. Tang, *Adv. Mater.*, 2011, **23**, 3298–3302.
- 25 S. Chen, H. Wang, Y. Hong and B. Z. Tang, *Mater. Horiz.*, 2016, **3**, 283–293.
- 26 Y. Cheng, C. Sun, X. Ou, B. Liu, X. Lou and F. Xia, *Chem. Sci.*, 2017, **8**, 4571–4578.
- 27 X. Shi, C. Y. Y. Yu, H. Su, R. T. K. Kwok, M. Jiang, Z. He, J. W. Y. Lam and B. Z. Tang, *Chem. Sci.*, 2017, **8**, 7014–7024.
- 28 D. Ding, R. T. K. Kwok, Y. Yuan, G. Feng, B. Z. Tang and B. Liu, *Mater. Horiz.*, 2015, **2**, 100–105.
- 29 Y. Yuan, S. Xu, C.-J. Zhang, R. Zhang and B. Liu, *J. Mater. Chem. B*, 2016, **4**, 169–176.
- 30 F. Meng, W. E. Hennink and Z. Zhong, *Biomaterials*, 2009, **30**, 2180–2198.
- 31 L. Jia, D. Cui, J. Bignon, A. Di Cicco, J. Wdzieczak-Bakala, J. Liu and M. H. Li, *Biomacromolecules*, 2014, **15**, 2206–2217.
- 32 P. Zhang, H. Zhang, W. He, D. Zhao, A. Song and Y. Luan, *Biomacromolecules*, 2016, **17**, 1621–1632.
- 33 W. Li, P. Zhang, K. Zheng, Q. Hu and Y. Wang, *J. Mater. Chem. B*, 2013, **1**, 6418.
- 34 L. Jia, Z. Li, D. Zhang, Q. Zhang, J. Shen, H. Guo, X. Tian, G. Liu, D. Zheng and L. Qi, *Polym. Chem.*, 2013, **4**, 156–165.
- 35 D. M. Townsend, K. D. Tew and H. Tapiero, *Biomed. Pharmacother.*, 2003, **57**, 145–155.
- 36 W. Cheng, G. Wang, X. Pan, Y. Zhang, B. Z. Tang and Y. Liu, *Macromol. Biosci.*, 2014, **14**, 1059–1066.
- 37 Y. Wang, M. Z. Lv, N. Song, Z. J. Liu, C. Wang and Y. W. Yang, *Macromolecules*, 2017, **50**, 5759–5766.
- 38 Z. K. Wang, L. Yang, Y. L. Liu, X. F. Huang, F. H. Qiao, W. Qin, Q. L. Hu and B. Z. Tang, *J. Mater. Chem. B*, 2017, **5**, 4981–4987.
- 39 Z. Long, M. Liu, R. Jiang, Q. Wan, L. Mao, Y. Wan, F. Deng, X. Zhang and Y. Wei, *Chem. Eng. J.*, 2017, **308**, 527–534.
- 40 X. Zhang, X. Zhang, B. Yang, M. Liu, W. Liu, Y. Chen and Y. Wei, *Polym. Chem.*, 2013, **4**, 4317.
- 41 X. Liu, Y. Chen, H. Li, N. Huang, Q. Jin, K. Ren and J. Ji, *ACS Nano*, 2013, **7**, 6244–6257.
- 42 R. Pan, G. Liu, Y. Li, Y. Wei, S. Li and L. Tao, *Nanoscale*, 2018, **10**, 8269–8274.
- 43 J. Zhang, X. Zheng, X. Hu and Z. Xie, *J. Mater. Chem. B*, 2017, **5**, 4470–4477.
- 44 N. Li, H. Yang, W. Pan, W. Diao and B. Tang, *Chem. Commun.*, 2014, **50**, 7473–7476.
- 45 Z. Wang, B. Xu, L. Zhang, J. Zhang, T. Ma, J. Zhang, X. Fu and W. Tian, *Nanoscale*, 2013, **5**, 2065–2072.
- 46 L. Jia, D. Cui, J. Bignon, A. Di Cicco, J. Wdzieczak-Bakala, J. Liu and M.-H. Li, *Biomacromolecules*, 2014, **15**, 2206–2217.
- 47 P. Zhang, H. Zhang, W. He, D. Zhao, A. Song and Y. Luan, *Biomacromolecules*, 2016, **17**, 1621–1632.
- 48 W. C. Wu, C. Y. Chen, Y. Tian, S. H. Jang, Y. Hong, Y. Liu, R. Hu, B. Z. Tang, Y. T. Lee, C. T. Chen, W. C. Chen and A. K. Y. Jen, *Adv. Funct. Mater.*, 2010, **20**, 1413–1423.
- 49 S. Chen, C. Zhang, G. Jia, J. Duan, S. Wang and J. Zhang, *Mater. Sci. Eng., C*, 2014, **43**, 330–342.
- 50 Q. Sun, T. Ishii, K. Kanehira, T. Sato and A. Taniguchi, *Biomater. Sci.*, 2017, **5**, 1014–1021.